

## [ISMT2021] Effect of parameters on penetration properties in butt welding of super duplex stainless steel using PAW-TIG heat source

Jun-Sub Yeo<sup>1</sup> • Moo-Keun Song<sup>2</sup> • Jong-Do Kim<sup>†</sup>

(Received November 8, 2021 : Revised November 26, 2021 : Accepted January 28, 2022)

**Abstract:** The materials that make up pipes of exhaust gas cleaning systems (EGCS) installed in ships must have remarkable corrosion-resistant properties. Austenitic stainless steel has been widely utilized for such pipes owing to its excellent corrosion resistance. Recently, the demand for super duplex stainless steel (SDSS) has increased, which exhibits higher strength, hardness, and corrosion resistance than austenitic stainless steel. In response to this demand, considerable research on the application of SDSS to pipes in ships should be conducted. In this study, keyhole welding based on the plasma arc welding (PAW) process, which does not require bevel or filler metal, was applied to the SDSS used for a sulfur oxide (SO<sub>x</sub>) EGCS in eco-friendly ships. A tungsten inert gas (TIG) welding heat source was included to increase the welding quality and durability. To examine the welding properties of SDSS, the penetration characteristics of the PAW and TIG heat sources affecting SDSS were analyzed. The effects of various process parameters in PAW–TIG hybrid tandem bead welding and butt welding of SDSS were also evaluated. The experimental results verified the effects of welding variables (e.g., welding current, voltage, and velocity) on the penetration depth and bead width. A mechanical test conducted on butt weldments confirmed the integrity of the weldments.

**Keywords:** Super duplex stainless steel, PAW, TIG, Butt welding, Mechanical test

### 1. Introduction

The interest in the harmful effects of air pollution on the environment and the human system has increased since the second half of the twentieth century. In response to such concerns, countries have strengthened air pollution control regulations in every field. The International Maritime Organization (IMO) adopted a protocol on the prevention of air pollution to reduce the amount of air pollutants emitted by ships, which came into effect in accordance with the established ratification and implementation processes [1]–[6].

The IMO designated certain regions significantly affected by air pollutants emitted by ships as emission control areas, and applied reinforced emission standards to these areas. An increasing number of countries have also initiated different emission regulations suited to their own circumstances [1]–[6].

In compliance with these regulations, several shipowners have recently installed exhaust gas cleaning systems (EGCSs). Pipes of such systems are made of various materials with excellent

corrosion resistance. Austenitic stainless steel is the most widely used material among the various types of stainless steel because of its excellent corrosion resistance. However, it was recently found that duplex stainless steel exhibits higher strength, hardness, and corrosion resistance. In this regard, studies on super duplex stainless steel (SDSS) that contain larger amounts of chromium, molybdenum, and nitrogen compared with general duplex stainless steel, are required [3]–[6].

In this study, keyhole welding was applied based on the plasma arc welding (PAW) process, which can get a greater welding part of fusion depth against fusion width and does not require bevel or filler metal, to perform bead welding and butt welding of SDSS used for sulfur oxide (SO<sub>x</sub>) EGCS in eco-friendly ships. Hybrid tandem welding based on a trailing tungsten inert gas (TIG) welding heat source, which has a wide fusion width and good fusion quality, was also utilized to prevent humping and undercutting on the bead surface.

Through these processes, the penetration characteristics of the

<sup>†</sup> Corresponding Author (ORCID: <http://orcid.org/0000-0002-2125-0426>): Professor, Division of Marine System Engineering, Korea Maritime & Ocean University, 727, Taejong-ro, Yeongdo-gu, Busan 49112, Korea, E-mail: [jdkim@kmou.ac.kr](mailto:jdkim@kmou.ac.kr), Tel: 051-410-4253

1 Senior Surveyor, Conformity Evaluation Center, Korean Register, E-mail: [jsyeo@krs.co.kr](mailto:jsyeo@krs.co.kr), Tel: 070-8799-8923

2 Researcher, Laser Advanced Machining Support Center, Korea Maritime & Ocean University, E-mail: [mksong@kmou.ac.kr](mailto:mksong@kmou.ac.kr), Tel: 051-410-4676

This is an Open Access article distributed under the terms of the Creative Commons Attribution Non-Commercial License (<http://creativecommons.org/licenses/by-nc/3.0>), which permits unrestricted non-commercial use, distribution, and reproduction in any medium, provided the original work is properly cited.

PAW and TIG heat sources affecting the SDSS were identified. Furthermore, the effects of the parameters during PAW–TIG hybrid tandem bead welding and butt welding of SDSS were evaluated.

## 2. Experimental Materials and Method

As the EGCS uses seawater to remove  $\text{SO}_x$ , its pipelines can corrode from the suction, cleaning, and discharge of seawater. In this study, the use of duplex stainless steel as a material for these pipelines was considered. Duplex stainless steel has high corrosion resistance owing to the changes in its microstructure caused by the insertion of a considerable amount of chrome and a small amount of nickel compared with general 12%-chrome stainless steel. In particular, SDSS has higher corrosion resistance and strength because it contains a larger amount of chrome, molybdenum, and nitrogen than general duplex stainless steel. **Table 1** presents the chemical composition of SDSS. SDSS with a thickness of 5 mm, which is the most widely applied to pipes in the fields of shipbuilding and marine engineering, was used to produce a 300 mm × 200 mm plate [3]–[10].

**Table 1:** Chemical composition of austenitic-ferritic steels [11]

UNS number	C Max.	Si Max.	Mn Max.	P Max.	S Max.	N	Cr	Cu	Mo	Ni
S32750	0.030	1.00	2.00	0.035	0.015	0.20–0.35	24.0–26.0	–	3.0–4.5	6.0–8.0

**Table 2:** Conditions of PAW process

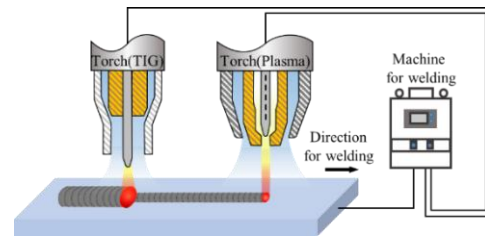
	$I$ (A)	$V$ (V)	$v$ (mm/min)	$G_s$	$Q_{gs}$ (l/min)	$D_{P-T}$ (mm)
PAW-bead	50	20	300	$\text{H}_2$ (7%) + Ar (93%)	10	300
	100	25	400			320
	150	27	500			340
	200	30	600			360
	250	33	700			380
	300	35	800			400
PAW-butt	200	20	450	$\text{H}_2$ (7%) + Ar (93%)	10	300
	250	25	500			
	300	30	550			

**Table 2** lists the various PAW conditions applied to bead welding and butt welding in this study. **Table 3** lists the TIG conditions with a fixed welding variable. As shown in **Figures 1** and **2**, complete penetration welding was conducted under the aforementioned PAW conditions. Then, TIG welding was performed to obtain a smooth upper bead surface. For bead welding in the

**Table 3:** Conditions of TIG process

	$I$ (A)	$V$ (V)	$v$ (mm/min)	$G_s$	$Q_{gs}$ (l/min)
TIG	235	18	500	$\text{H}_2$ (7%) + Ar (93%)	25

PAW process, the welding current, welding voltage, welding velocity, and distance between heat sources were applied as variables. For butt welding in the PAW process, the welding current, welding voltage, and welding velocity were applied as variables. In this experiment,  $G_s$  and  $Q_{gs}$  represent the shield gas type and shield gas flow rate, respectively. The distance between heat sources ( $D_{P-T}$ ) refers to the distance between the PAW and TIG heat sources [12][13].

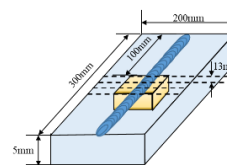


**Figure 1:** PAW–TIG hybrid tandem welding system

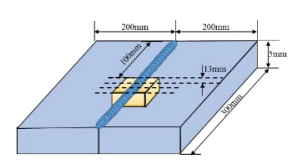


**Figure 2:** Experimental setup for hybrid tandem process

(a) Bead welding



(b) Butt welding



**Figure 3:** Sampling position of welding

Bead welding and butt welding of the SDSS plate were performed. To stably obtain a welded specimen, the original plate was cut at intervals of 13 mm from a point 100 mm away from the starting point of welding, as shown in **Figure 3**. The width and depth of the bead at the weldments of the cut specimen were measured, and changes in the welding shape according to the welding variables were observed. The mechanical properties of

the weldments were verified by hardness measurements and tensile and bending tests.

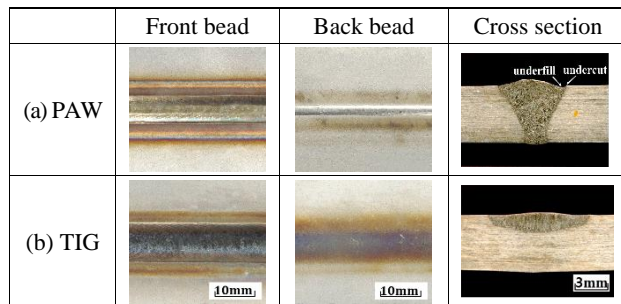
### 3. Results and Discussion

#### 3.1 Bead welding properties according to conditions of PAW-TIG hybrid tandem welding of SDSS

In this experiment, welding was performed separately using different heat sources to verify the penetration characteristics of PAW and TIG welding. **Figure 4** shows the bead surface and cross-section of each weldment.

Complete penetration welding was performed at the PAW weldments, as shown in **Figure 4(a)**, despite the narrower bead than that at the TIG weldments in **Figure 4(b)**. However, undercut and underfill defects were partially observed at the PAW weldments in **Figure 4(a)** [14][15]. The bead surface at the TIG weldments was more stable and wider than that at the PAW weldments. Based on these results, hybrid tandem welding combining both heat sources was conducted to ensure higher stability and penetration depth of the bead.

Then, bead welding was conducted under fixed TIG welding conditions and varying PAW conditions to verify the hybrid tandem welding characteristics.

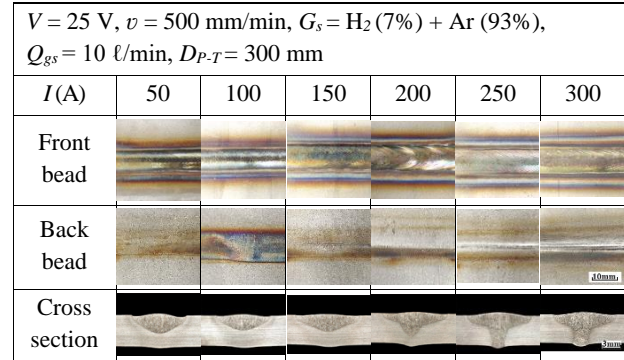


**Figure 4:** Photographs of bead appearance and cross-section in PAW and TIG processes

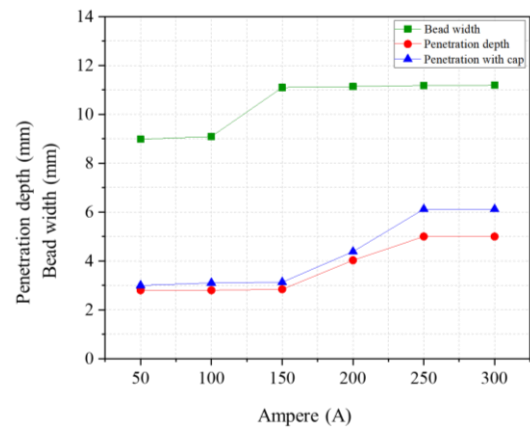
##### 3.1.1 Effect of the welding current and voltage

The welding current and voltage as variables significantly affect the welding conditions, such as the degree of fusion and penetration depth. An experiment was conducted to analyze the effects of PAW-based current and voltage conditions on the PAW-TIG hybrid tandem welding of SDSS.

The effects of current ( $I$ ) changes during the PAW process, i.e., 50, 100, 150, 200, 250 and 300 A, respectively, were examined, as shown in **Figures 5** and **6**. The increase in the current led to an increase in the heat input; the width of the front bead and the penetration depth also tended to increase. Keyhole welding was

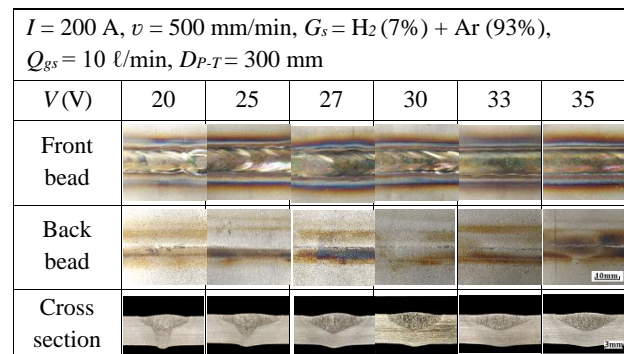


**Figure 5:** Photographs of bead appearance and cross-section with current



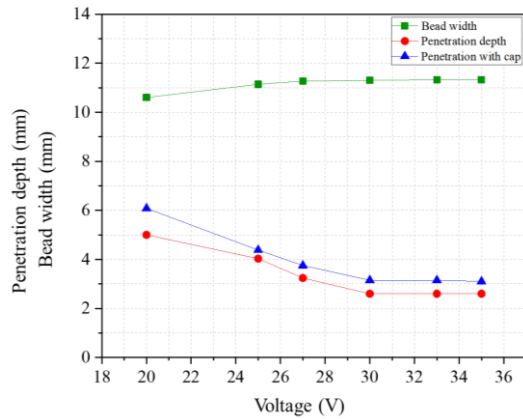
**Figure 6:** Variation of bead width, penetration with cap, and penetration depth with current

performed at a current of 200 A or higher, and complete penetration welding was performed at a current of 250 A or higher. In addition, penetration with a cap, which represents the distance between the top and bottom welding reinforcements, showed an increasing trend at 150–250 A.



**Figure 7:** Photographs of bead appearance and cross-section with voltage

The voltage ( $V$ ) in the PAW process was varied from 20 to 35 V to analyze its effect on the welding. **Figures 7** and **8** show the



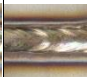





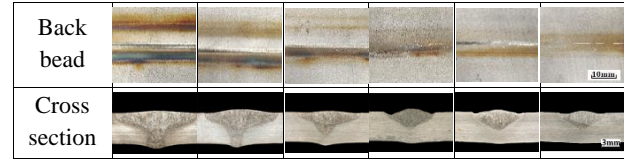
**Figure 8:** Variations of bead width, penetration with cap, and penetration depth with voltage

front and back beads and cross-sections of the weldments according to voltage changes. It was found that an increase in voltage slightly increased the width of the beads, but did not significantly affect the beads. In contrast, the penetration depth tended to decrease as the voltage increased in the cross-sections of the weldments. This result was obtained because an increase in the welding voltage indicates an increase in the distance between the parent material and electrode. As a result, keyhole welding was performed at a voltage of up to 25 V. The desired penetration depth was not achieved at voltages above 25 V.

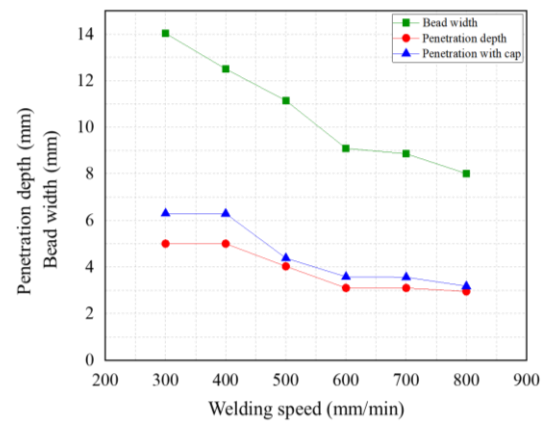
### 3.1.2 Effect of welding velocity by electrode movement

Similar to the welding current and voltage, the welding velocity is another variable that affects the amount of heat input, the range of the heat-affected zone, and the cooling velocity at the weldment. Thus, the welding velocity ( $v$ ) was varied from 300 to 800 mm/min to analyze its effects, as shown in **Figures 9** and **10**. The increase in the welding velocity led to a decrease in the heat input, bead width, and penetration depth. In particular, the bead width was significantly reduced. Consequently, penetration welding was performed at a welding velocity of up to 500 mm/min. Complete penetration did not occur at welding velocities above 500 mm/min.

$I = 200 \text{ A}$ , $V = 25 \text{ V}$ , $G_s = \text{H}_2 (7\%) + \text{Ar} (93\%)$ , $Q_{gs} = 10 \text{ l/min}$ , $D_{P-T} = 300 \text{ mm}$						
$v$ (mm/min)	300	400	500	600	700	800
Front bead						



**Figure 9:** Photographs of bead appearance and cross-section with welding velocity by electrode movement













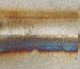
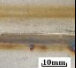






**Figure 10:** Variation of bead width, penetration with cap, and penetration depth with welding speed

### 3.1.3 Effect of distance between PAW and TIG heat sources

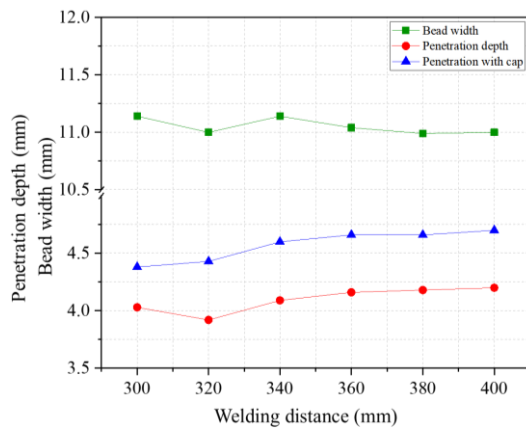
In an experiment on the application of the PAW–TIG hybrid tandem welding system, the distance between the PAW system and TIG welding system was applied as a variable. The distance between heat sources during hybrid welding significantly affected the behavior of the melting pool. Thus, the effect of the distance between the PAW electrodes (the forward heat source) and TIG (the trailing heat source) was verified in this experiment. The distance between heat sources ( $D_{P-T}$ ) was varied as 300, 320, 340, 360, 380, and 400 mm, respectively, considering the interference caused by experimental equipment. **Figures 11** and **12** show the analytical results. The increase in the distance between the heat sources from 300 mm to 400 mm did not significantly affect the width of the front bead, penetration depth, and penetration depth applying upper and bottom caps. In general, the welding efficiency increased because of the interactions between both heat sources during the hybrid welding process. However, the effect of the distance between heat sources was determined to be negligible in this experiment because of the following reasons. First, PAW (the forward heat source) determines the penetration depth, whereas TIG welding (the trailing heat source) determines the stability of the bead surface. Thus, neither source affected



each other. Second, welding was performed under the condition that the distance between the heat sources was at least 300 mm

$I = 200\text{ A}$ , $V = 25\text{ V}$ , $v = 500\text{ mm/min}$ , $G_s = \text{H}_2 (7\%) + \text{Ar} (93\%)$ , $Q_{gs} = 10\text{ l/min}$						
$D_{P-T}$ (mm)	300	320	340	360	380	400
Front bead						
Back bead						
Cross section						

**Figure 11:** Photographs of bead appearance and cross-section with distance between PAW and TIG



**Figure 12:** Variation of bead width, penetration with cap, and penetration depth with distance between PAW and TIG


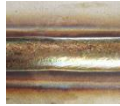
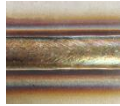
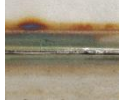

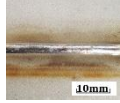



because of the interference of the experimental equipment. That is, welding based on the trailing heat source was performed after the fusion pool by the forward heat source was coagulated. As a result, neither source was expected to have a significant effect on the other. Thus, in the subsequent butt welding, a hybrid tandem welding experiment was performed in which the distance between the heat sources was fixed at 300 mm.

### 3.2 Butt welding characteristics according to conditions during PAW-TIG hybrid tandem welding of SDSS

#### 3.2.1 Effect of the welding current and voltage


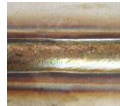
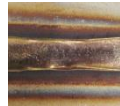


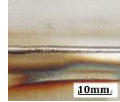



Based on the results of the bead welding experiment, it was confirmed that the optimal conditions of PAW include a current ( $I$ ) of 250 A, voltage ( $V$ ) of 25 V, welding velocity ( $v$ ) of 500 mm/min, and distance ( $D_{P-T}$ ) of 300 mm between the heat sources of PAW and TIG. A butt welding experiment based on the hybrid

tandem heat sources of PAW and TIG was conducted to examine the effects of each parameter.

$V = 25\text{ V}$ , $v = 500\text{ mm/min}$ , $G_s = \text{H}_2 (7\%) + \text{Ar} (93\%)$ , $Q_{gs} = 10\text{ l/min}$ , $D_{P-T} = 300\text{ mm}$			
$I$ (A)	200	250	300
Front bead			
Back bead			
Cross section			

**Figure 13:** Photographs of bead appearance and cross-section with current by butt welding

To analyze the effect of the change in the current, the current ( $I$ ) in the PAW process was varied to 200, 250, and 300 A, respectively, as shown in **Figure 13**. When the current increased from 200 to 300 A, the heat input increased. Accordingly, the width of the front bead, penetration depth, and penetration depth applying upper and bottom caps tended to increase. In addition, the cross-sections of the weldments were analyzed. The results showed that keyhole welding and complete penetration were achieved with the formation a stable bead surface at 200, 250, and 300 A. The results verify that a current of 250 A is the optimal condition to minimize the heat input; above the critical condition, complete penetration was achieved.

$I = 250\text{ A}$ , $v = 500\text{ mm/min}$ , $G_s = \text{H}_2 (7\%) + \text{Ar} (93\%)$ , $Q_{gs} = 10\text{ l/min}$ , $D_{P-T} = 300\text{ mm}$			
$V$ (V)	20	25	30
Front bead			
Back bead			
Cross section			






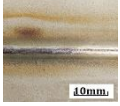



**Figure 14:** Photographs of bead appearance and cross-section with voltage by butt welding

The effects of voltage changes were examined at 20, 25, and 30 V, respectively, as shown in **Figure 14**. In contrast to the increase

in the current, the increase in the voltage led to a decrease in the width of the front bead, penetration depth, and penetration depth applying upper and bottom caps. In addition, both keyhole welding and complete penetration were performed under all conditions. At the comparatively low voltage of 20 V, excessive penetration was observed in the bead shape owing to the shortened distance between the parent material and electrode. At the comparatively high voltage of 30 V, plasma welding was narrow in terms of width owing to shallow penetration. Thus, the voltage of 25 V, which is below the critical condition of complete penetration, was determined to be the optimal welding voltage.

### 3.2.2 Effect of welding velocity by electrode movement

An experiment was conducted to examine the effect of the welding velocity ( $v$ ) of 450, 500, and 550 mm/min, respectively. **Figure 15** shows the experimental results. As the welding velocity increased, the heat input decreased. Accordingly, the bead width, penetration depth, and penetration depth applying upper and bottom caps tended to decrease. However, the bead width was significantly wide owing to the excessive heat input at the welding velocity of 450 mm/min. The high welding velocity of 550 mm/min led to an underfill defect. Therefore, 500 mm/min was determined to be the optimal welding velocity during PAW–TIG hybrid tandem butt welding.

$I = 250 \text{ A}$ , $V = 25 \text{ V}$ , $G_s = \text{H}_2 (7\%) + \text{Ar} (93\%)$ , $Q_{gs} = 10 \text{ l/min}$ , $D_{P-T} = 300 \text{ mm}$			
$v(\text{mm/min})$	450	500	550
Front bead			
Back bead			
Cross section			

**Figure 15:** Photographs of bead appearance and cross-section with welding velocity by electrode movement by butt welding

## 3.3 Mechanical properties of weldments during PAW–TIG hybrid tandem butt welding of SDSS

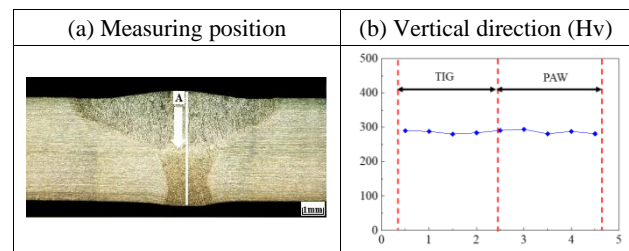
The integrity of the butt weldments based on hybrid tandem heat sources was analyzed by measuring the hardness distribution in the weldments and conducting tensile and bending tests. The mechanical properties of the parent materials are listed in **Table 4**.

**Table 4:** Mechanical properties of austenitic-ferritic steels

UNS number	Hardness	Tensile strength	Bending test
S32750	Max. 327 Hv	800–1,000 MPa	No crack

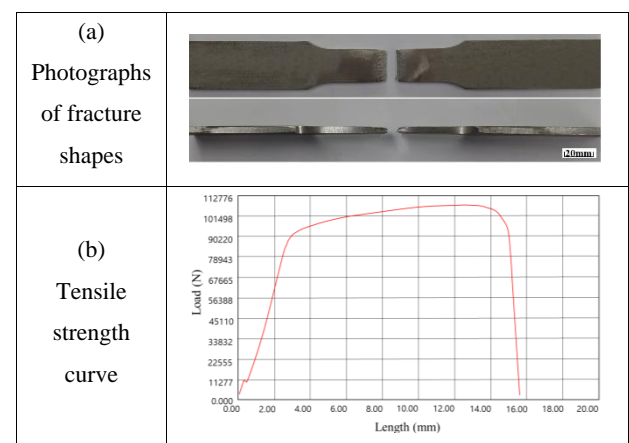
### 3.3.1 Hardness distribution

As shown in **Figure 16**, the hardness of the weldments was measured from the TIG weldments located at the upper parts, to the PAW weldments located at the lower parts, along the direction of depth. The mean hardness in the TIG and PAW areas were calculated as 286 Hv and 287 Hv, respectively, which are similar to each other. The hardness of the weldment by hybrid tandem welding was lower than that of the parent material by a certain degree. However, this part was evaluated as an appropriate weldment as the hardness value satisfied the standard for the UNS S32750 material.



**Figure 16:** Hardness distribution for butt weldment

### 3.3.2 Tensile test



**Figure 17:** Photographs of fracture shapes and tensile strength curve for butt weldment

**Figure 17** shows the results of the tensile test conducted on three welding specimens by applying hybrid tandem heat sources according to EN ISO 6892-1. The tensile test involved subjecting a test piece to strain by tensile force, generally to fracture, to determine the mechanical properties defined in the EN ISO 6892-1

standard. The test was carried out at room temperature between 10 °C and 35 °C, unless otherwise specified. In the test, the mean tensile strength was calculated to be 870 MPa, which satisfied the standard for tensile strength in UNS S32750 despite the fracture of weldments. This result verifies the integrity of the weldments [16].

### 3.3.3 Bending test

**Figure 18** shows the result of the bending test conducted on weldments, which fulfilled the EN ISO 5173 under EN 10217-7 standards. The absence of welding defects (e.g., porosities and cracks) indicates that the standard for the bending test according to the EN 10217-7 specification was met [17].



**Figure 18:** Result of bending test for butt weldment

## 4. Conclusions

In this study, the PAW-TIG hybrid tandem welding of SDSS with a thickness of 5 mm was conducted. The SDSS was applied as a material for an SO<sub>x</sub> EGCS in an eco-friendly ship, and its welding properties were analyzed. The results obtained according to the various processing variables are as follows:

- (1) Bead welding was conducted based on the PAW heat source ( $I = 200$  A,  $V = 25$  V,  $v = 500$  mm/min) and TIG welding heat source ( $I = 235$  A,  $V = 18$  V,  $v = 500$  mm/min). The experimental results showed that complete penetration occurred at the PAW weldments. The penetration depth was shallow at the TIG weldments; however, the bead surface was stable and wide.
- (2) PAW-TIG hybrid tandem welding of the bead was conducted under the conditions of fixed TIG welding variables and adjusted main PAW processing variables. The experimental results showed that the increase in the welding current increased in the bead width and penetration depth. The increase in the voltage reduced the penetration depth but did not significantly affect the bead width. When the welding velocity increased, the heat input decreased. Accordingly, the bead width and penetration depth also decreased. However, it is thought that more noticeable

changes can be observed if complete control of the surrounding environment is implemented and subdivided, and a wide range of variables are set during the experiment.

- (3) The distance between the heat sources was established as a variable, and its effects on the welding properties were analyzed. The analytical results indicate that this variable did not affect the bead width nor the penetration depth. This result was obtained because in the fusion pool by PAW, the forward heat source was coagulated before it was affected by TIG (the trailing heat source).
- (4) The properties of hybrid tandem butt welding based on PAW and TIG heat sources tended to be similar to those of hybrid tandem bead welding. The most sound weldment was obtained under the following PAW conditions:  $I = 250$  A,  $V = 25$  V, and  $v = 500$  mm/min.
- (5) The mechanical properties of the weldments were analyzed through hardness measurements, tensile tests, and bending tests. The analytical results verified the integrity of the weldments.

## Acknowledgement

This paper is an expanded version of the proceeding paper entitled “Effect of Parameters on Penetration Properties in Butt Welding using PAW-TIG Heat Source with Super Duplex Stainless Steel” presented at the KOSME ISMT 2021.

## Author Contributions

Conceptualization, J. S. Yeo; Methodology, J. S. Yeo and J. D. Kim; Formal Analysis, J. S. Yeo; Data Curation, J. S. Yeo and M. K. Song; Writing-Original Draft Preparation, J. S. Yeo and M. K. Song; Writing-Review & Editing, J. S. Yeo and J. D. Kim; Supervision, J. D. Kim.

## References

- [1] S. Jo, A Study on Air Pollutant Emission Characteristics of Ships by Vessel Speed Reduction, Master Thesis, Department of Marine Engineering, Korea Maritime and Ocean University, Korea, 2020 (in Korean).
- [2] I. Park, *et al.* “A study on corrosion of distance piece on Exhaust Gas Cleaning Systems (EGCS) discharge waterline,” *Journal of Advanced Marine Engineering and Technology*, vol. 44, no. 6, pp. 453-456, 2020.

- [3] Official journal of the European Union, "Directive 2014/90/EU of the European parliament and of the council of 23 July 2014 on marine equipment and repealing council Directive 96/98/EC," European Union, 2014/90/EU, 2014.
- [4] Official journal of the European Union, "Regulations commission implementing regulation (EU) 2020/1170 of 16 July 2020 on design, construction and performance requirements and testing standards for marine equipment and repealing Implementing Regulation (EU) 2019/1397," European Union, (EU)2020/1170, 2020.
- [5] IMO, "Resolution MEPC.184(59) adopted on 17 July 2009 \_2009 guidelines for exhaust gas cleaning systems," IMO, MEPC.184(59), 2009.
- [6] IMO, "Resolution MEPC.259(68) adopted on 15 May 2015 \_2015 guidelines for exhaust gas cleaning systems," IMO, MEPC.259(68), 2015.
- [7] J. H. Lee, *et al.*, Understanding of Stainless Steel, Myungjin Publishing Company, 2016 (in Korean).
- [8] Korean Register, Exhaust Gas Cleaning Systems Technical Information for Ship-Owner and Surveyor, Korean Register, 2018 (in Korean).
- [9] Korean Register Technology Team, Ship-Owner's Guide to Respond for Enhanced Global SOx Regulatory, Korean Register, 2018 (in Korean).
- [10] J. -A. Jeong, *et al.*, "Electrochemical and on-site tests for the application of cathodic protection on the inner surface of seawater pipes," Journal of Advanced Marine Engineering and Technology, vol. 43, no. 8, pp. 610-617, 2019.
- [11] BSI Standards Publication, "Welded steel tubes for pressure purposes – Technical delivery conditions- Part 7: Stainless steel tubes," EN, EN 10217-7(2014), 2014.
- [12] W. -H. Choe, *et al.*, "Application of plasma arc welding for anti-corrosive material with high molybdenum content," Journal of Welding and Joining, vol. 38, no. 3, pp. 333-338, 2020 (in Korean).
- [13] S. Jung, *et al.*, "A study for the welding condition optimization using response surface method in TIG butt welding of A6061 aluminum alloy," Journal of Welding and Joining, vol. 36, no. 3, pp. 1-7, 2018 (in Korean).
- [14] The Korean Welding and Joining Society, "III. Process and Heat processing," Welding and Joining Manual, 4<sup>th</sup> Edition: GS Interservice Publishing Company, 2007 (in Korean).
- [15] J. D. Kim, *et al.*, Familiar Welding and Joining Engineering, 2<sup>nd</sup> Edition: Dasom Publishing Company, 2010 (in Korean).
- [16] BSI Standards Publication, "Metallic materials - Tensile testing - Part 1: Method of test at room temperature," EN, EN ISO 6892-1(2016), 2016.
- [17] BSI Standards Publication, "Destructive tests on welds in metallic materials - Bend tests," EN, EN ISO 5173(2010)+A1(2011), 2011.
- [18] J. -S. Yeo, M. -K. Song, and J. -D. Kim, "Effect of parameters on penetration properties in butt welding using PAW-TIG heat source with super duplex stainless steel," Proceedings of the International Symposium on Marine Engineering and Technology 2021, Korea, Busan, 2021.